

# OnePerc: A Randomness-aware Compiler for Photonic Quantum Computing

Hezi Zhang<sup>1</sup>, Jixuan Ruan<sup>1</sup>, Hassan Shapourian<sup>2</sup>, Ramana Rao Kompella<sup>2</sup>, Yufei Ding<sup>1</sup>

<sup>1</sup>University of California, San Diego

<sup>2</sup>Cisco Quantum Lab

## Abstract

The photonic platform holds great promise for quantum computing. Nevertheless, the intrinsic probabilistic characteristics of its native fusion operations introduces substantial randomness into the computing process, posing significant challenges to achieving scalability and efficiency in program execution. In this paper, we introduce a randomness-aware compilation framework designed to concurrently achieve scalability and efficiency. Our approach leverages an innovative combination of offline and online optimization passes, with a novel intermediate representation serving as a crucial bridge between them. Through a comprehensive evaluation, we demonstrate that this framework significantly outperforms the most efficient baseline compiler in a scalable manner, opening up new possibilities for realizing scalable photonic quantum computing.

## 1 Introduction

Photonic platform holds great promise for universal quantum computing due to the unique advantages of photonic qubits [1, 2], including their great scalability, long coherence time and easy integration with quantum networks. In addition to the experimental demonstration of quantum supremacy on photonic systems [3–5], Xanadu [6] has released their programmable nanophotonic chips that can serve as a new testbed, while PsiQuantum [7] has proposed their technology roadmap towards one million qubits using silicon photonics.

Photonic quantum computing differs from other platforms such as superconducting [8], ion trap [9] and neutral atoms [10], as it is scaled up by a probabilistic operation known as *fusion* [7]. This probabilistic feature comes intrinsically from the degeneracy in fusions’ outputs for different input states, bringing significant randomness to the computing process. On the hardware side, improvement of fusion success probability to a high value requires an impractical amount of ancillary resources [11, 12]. On the software side, this randomness is not taken into consideration by existing software infrastructures for the circuit-based programming model [13], (e.g., Qiskit [14], Tket [15]), as photonic systems adopt a different computing model, which is known as measurement-based quantum computation (MBQC) or one-way quantum computation (1WQC) [16, 17].

Recently, as an initial effort towards efficient photonic MBQC, a compilation framework OneQ [18] has been proposed to significantly reduce the number of required fusions and the overall program execution time. However, it overlooks the severe randomness introduced by fusion failures, simply assuming that fusions always succeed. As a compiler, OneQ translates the construction of a program-specific entangled state called *graph state* [17] (Fig. 1(a)) into a fusion pattern between the small entangled *resource states* [7] available on the hardware (Fig. 1(b)). However, when fusion failures occur in real-time execution, as illustrated in Fig. 1(b), the resulting state becomes a random graph state deviating from the target structure. Thus the execution needs to be retried until success, which is non-scalable given that a practical fusion success probability in the near term is merely around 75% [11, 12]. From now on, we will refer to the graph states required by programs as *program graph states* and those generated by fusions as *physical graph states*.

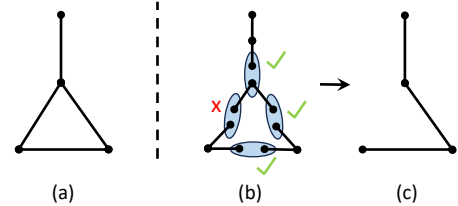


**Figure 1.** Randomness brought by fusion failures on a photonic quantum hardware with 3-qubit resource states.

The objective of this paper is to present a scalable and efficient compilation framework capable of effectively handling fusion failures in the computing process. This is intuitively a hard problem. Firstly, with a failure rate as high as 25%, it seems impossible to ensure the formation any specific entanglement structure among the photonic qubits. Secondly, failed entanglements such as the disconnected edges in Fig. 1 cannot be recovered since the photons involved in a fusion are completely destroyed by the fusion. Thirdly, the limited lifetime of photons refuses the execution of over-complex algorithms in real-time, as photons are prone to an increasing loss rate with prolonged storage time in fibers [19].

Fortunately, there are some nice features of fusions and graph states that we can leverage. Firstly, fusion failures are heralded [20], allowing real-time awareness and enabling

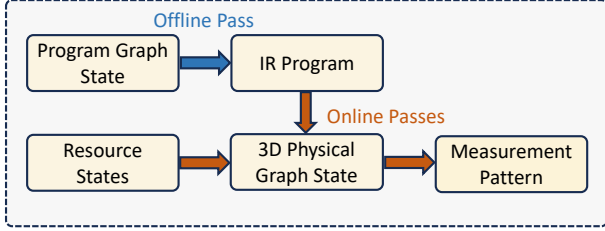


**Figure 2.** High-level design of OnePerc.

the incorporation of classical feed-forward [20–22] to adjust subsequent operations based on prior fusion outcomes. Secondly, when the fusion success probability exceeds a threshold, the resulting physical graph state contains a long-range-connected component with a high probability. This widely studied phenomena, known as percolation [23–25], plays a crucial role in providing viable computing resource, inspiring our framework’s name, OnePerc (one-way quantum computing based on percolation). Thirdly, a random graph state can be reshaped into any subgraph of it by eliminating the redundant qubits, which can be achieved by measuring them out in  $Z$ -bases [16].

However, leveraging these features is highly non-trivial. In addition to the absence of a generic fusion strategy among general resource states for achieving percolation and the structural mismatch between the high-level program graph state and the low-level random physical graph state, we need to always keep in mind the limited time for real-time passes. Specifically, the process associated with the formation of long-range connectivity and the reshaping of the random physical graph state both need to be carried out in real-time, leading to a high demand on their lightweight design. This results in a conflict between the real-time scalability and the program execution efficiency, as a sophisticated optimization for program execution requires complex algorithms that are not feasible in real-time.

To this end, we propose a randomness-aware compiler designed to efficiently scale up quantum computing on photonic systems, as illustrated in Fig. 2. Our framework achieves concurrent real-time scalability and program execution efficiency through the combination of an online pass and an offline pass. The online pass handles real-time randomness in a scalable manner through percolation and reshaping. In particular, it provides a generic fusion strategy for various resource states and mitigates the structural mismatch between program and physical graph states by enabling the abstraction of a virtual hardware. Motivated by the features of this virtual hardware, we propose a *FlexLattice* intermediate representation (IR), which preserves the high-level program information and provides maximal optimization space supported by the hardware. This allows offline passes to optimize the program execution by transforming the program to an efficient IR program, with the IR program translated to a low-level instruction set to guide real-time operations.

Our contributions in this paper are summarized as follows:

- We propose a randomness-aware compilation framework for photonic quantum computing through an innovative combination of online and offline passes, which are bridged by a novel *FlexLattice* IR facilitated with a low-level instruction set.
- The online pass handles real-time randomness in a scalable manner by enabling long-range connectivity formation among general resource states and efficient reshaping of the random long-range connected computing resource.
- The *FlexLattice* IR provides programs with a maximal optimization space supported by the underlying hardware, allowing for the introduction of a sophisticated offline pass to improve the efficiency of program execution.
- Our evaluation demonstrates a significant outperformance over the efficient baseline in a scalable manner, implying a first-time concurrent achievement of scalability and efficiency in compilation of photonic quantum computing.

## 2 Background and Motivation

### 2.1 Photonic MBQC

Photonic systems are particularly suitable for MBQC [26], a conceptually distinct computing paradigm from the circuit model. In MBQC, computation is driven by single-qubit projective measurements, rather than 1-qubit and 2-qubit gates, on an initial entangled state called *graph state*, whose graph structure  $G = (V, E)$  is determined by the quantum program [17], as exemplified in 3(a). Specifically, a graph state consists of qubits located on  $G$ , formally defined as the eigenstates of operator

$$s = X_i \bigotimes_{j \in n_i} Z_j, \quad \forall i \in V$$

where  $n_i$  is the set of neighboring qubits of  $i \in V$ . The measurement basis of each qubit is predetermined by the quantum program, known as a *measurement pattern*, but are subject to a real-time adjustment according to the measurement outcomes of prior qubits. This feed-forward is used to address the non-determinism of measurement outcomes.

The feasibility of photonic MBQC has been demonstrated with various quantum algorithms on photonic qubits. For instance, Grover’s algorithm achieved 0.9 fidelity on a 4-photon 4-qubit graph state [27], while the Deutsch-Jozsa algorithm reached 0.96 fidelity on a 6-qubit graph state [28]. In addition, Simon’s algorithm was successfully applied to a five-qubit cluster state for period-finding[29]. Notably, the photonic platform is rapidly scaling up with integrated waveguides and optical chips [30–34], enabling the realization of a programmable optical processor [6].

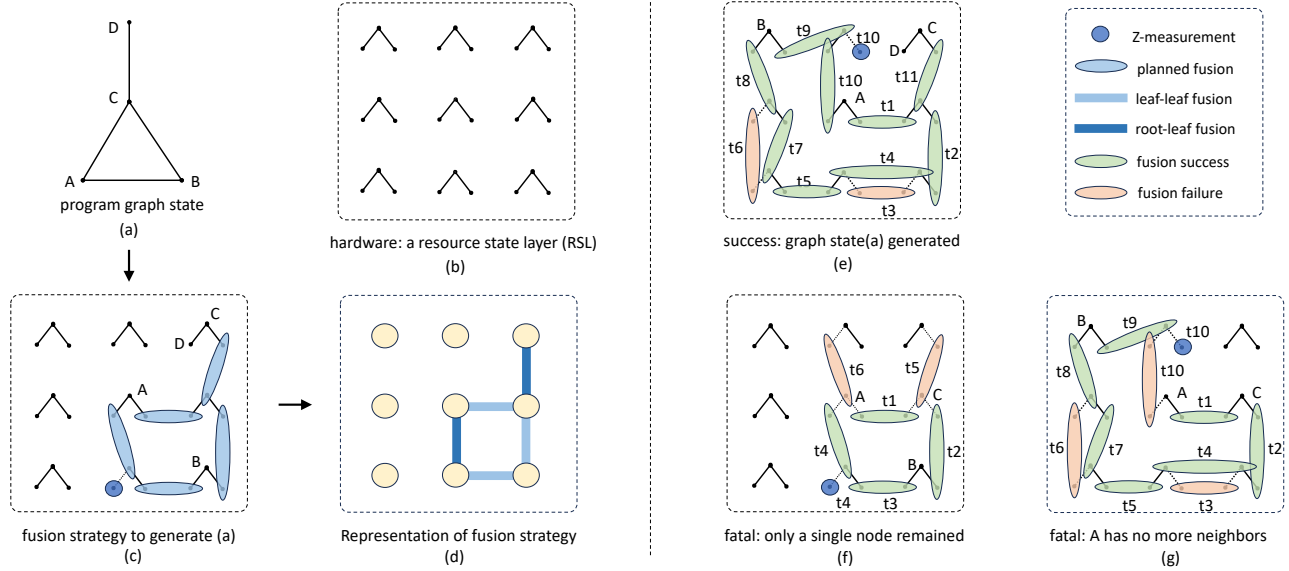


Figure 3. Why OneQ does not work.

## 2.2 Realistic Hardware

Practical photonic hardware scales up by creating small *resource states*, e.g., 4-qubit, 6-qubit graph states, and connecting them through *fusions* [7]. In particular, identical resource states are periodically generated by an array of *resource state generators* (RSG) every cycle, with those generated in the same RSG cycle forming a resource state layer (RSL), as depicted by Fig. 3(b). These resource states are merged probabilistically into larger graph states through (type II [20]) fusions, which are concurrent measurements of  $X \otimes Z$  and  $Z \otimes X$  on two photonic qubits from different resource states. Resource states on the same RSL can fuse with their neighbors, as shown in Fig. 3(c), by a spatial routing of photons, while those on different RSLs generated by the same RSG can fuse with each other by a temporal routing that controls photons' arrival times at measurement devices.

With the advanced integrated silicon photonics, hardware components described above can operate on the scales of GHz clock rates [35–37], leading to a time scale  $\sim 1$  ns for RSG cycles. Spatial routing can be adjusted in every RSG cycle with switches, while temporal routing can be achieved by temporarily storing photonic qubits in a high-capacity quantum memory known as *delay lines*, which can be realized with current optical fiber technology. With a low transmission loss rate of  $< 5\%$  per km [19], photons can have a lifetime of around 5000 RSG cycles in the delay lines. Moreover, the size of RSL is not completely constrained by the number of RSGs, but can be extended by leveraging the tradeoff between spatial and temporal fusions [38], with the 5000-cycle photon lifetime allowing a  $5000\times$  extension at most.

However, as the key operation for merging resource states, fusions are intrinsically probabilistic. By allowing two ancilla

photons, their success probability can be practically boosted to 75% [11, 12]. While no conceptual limit has been found yet, so far the maximum known success probability attainable using linear optics is 78% with 8 ancilla single photons [11]. Reaching a higher success probability not only requires a larger number of ancilla photons but also require the ancilla photons to be entangled. For example, it would take 30 ancilla entangled photons to reach a probability over 95% [12].

## 2.3 Motivating Example

Previous work has proposed OneQ [18], an efficient compilation framework for photonic MBQC. We will show that a straightforward adaption of OneQ is insufficient to yield a scalable compiler in the presence of fusion failures.

**OneQ + Retry.** Fig. 3(c) illustrates OneQ's strategy with an example of generating a graph state in Fig. 3(a) from a single RSL depicted in Fig. 3(b), with the strategy represented more compactly by Fig. 3(d). To handle real-time randomness, a straightforward adaption is to introduce a retry mechanism. For example, the strategy in Fig. 3(c) can result in a dynamic implementation in Fig. 3(e) according to the fusion successes and failures (green and red ellipses), with these fusions performed sequentially, from  $t_1$  to  $t_{11}$ . If a fusion, such as  $t_3$ , fails, we retry the fusion using another two qubits at  $t_4$ , and the same approach is applied to  $t_6$  and  $t_7$ . This allows us to successfully generate the graph state in Fig. 3(a).

However, it is worth noting that some fatal failures may necessitate the retrieval of the entire compilation. For example, in Fig. 3(f), the triangular structure ABC is successfully generated from  $t_1$  to  $t_4$ , but subsequent failures at  $t_5$  and  $t_6$  deplete the qubits in ABC, only leaving the isolated qubit B. In Fig. 3(g), a 5-qubit linear graph state forms from  $t_1$  to  $t_{11}$ ,

which provides the potential for generating the triangle ABC if the fusion at t11 succeeds in fusing the two qubits at the line ends. Unfortunately, this fusion fails and consumes the last neighboring resource state of qubit A (except C), leaving A with no chance to fuse with other qubits.

**Critical Issues.** From this example, we can find some critical issues of this dynamic retry mechanism. First, adapting to prior fusion outcomes necessitates a sequential execution of fusions. This considerably extends the processing time for each resource state layer (RSL), resulting in a time inefficiency as subsequent RSLs must wait for the completion of the current one. Second, since the decision-making process for responding to prior fusions occurs in real time, this extended processing time could exceed the limited lifetime of photons, especially for large RSLs. This would result in substantial photon loss, compromising the overall fidelity as computing scales up. Third, the frequent retries in real-time implementation lead to significant deviations from the planned strategy in Fig. 3(c). This undermines the benefits of the proactive planning, eroding the efficiency achieved by the mapping strategy of OneQ.

### 3 Overview

Tolerating randomness in the compilation while maintaining efficiency presents a significant challenge. To address this, we propose an innovative framework that achieves scalability and efficiency simultaneously through a synergy of online and offline passes. The online pass prioritizes the real-time scalability by maximizing the concurrency among fusions and the parallelism of the algorithm for decision making. The offline pass focuses on the efficient deployment of high-level program graph states onto the randomness-eliminated computing resource guaranteed by the online pass. The bridge between the online and offline passes is established through an intermediate software layer positioned between the low-level physical layer and the high-level program layer. This motivates a novel FlexLattice IR, along with an instruction set supported by the online pass and fulfilling the requirements of the offline pass.

To provide a concise overview, we exemplify the compilation flow by compiling the program graph state in Fig. 4(a) onto the hardware in Fig. 4(b), which is 3 layers of that in Fig. 3(b). Indeed, while Fig. 3(b) depicts only a single RSL, the incorporation of additional layers is both allowed and necessary for larger graph states. Steps (b)→(d)→(c) demonstrate the online pass, while step (a)→(c) illustrates the offline pass. In the online pass, fusions are conducted concurrently in a predetermined pattern (Fig. 4(d)) without individual retries of the failed ones, which eliminates the necessity for sequential operations. This results in a physical graph state with a random 2D structure, which is then reshaped to a program-agnostic  $2 \times 1$  lattice (Fig. 3(c)), characterized by a regular structure to enhance real-time efficiency. When the fusion

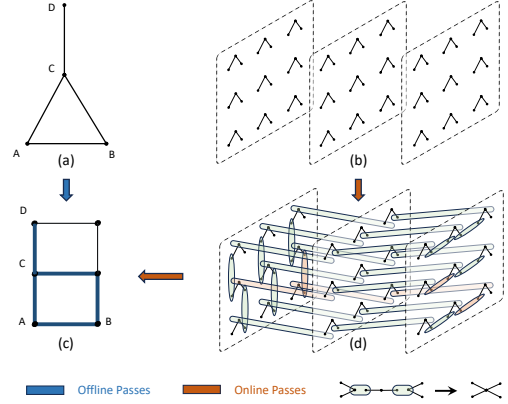


**Figure 4.** Overview of the compilation flow.

success probability exceeds the percolation threshold, this reshaping process attains near-deterministic success as the RSL size increases. This eliminates the necessity for repetitive retries of the entire compilation. With this determinism, the offline pass can be employed to improve the efficiency by mapping the program graph state compactly onto the  $2 \times 1$  lattice (bold blue lines in Fig. 3(c)).

Note that the compilation of general programs can be considerably more intricate than the example presented here. First, the fusion strategy among resource states is more complex than Fig. 4(d). Specifically, it enables the formation of a 3D structure rather than 2D, being adaptable to various resource states and allowing pipelined feed-forward with a small overhead. Second, the complexity of the reshaping algorithm is carefully reduced to enhance its real-time scalability. This is achieved by improving the parallelism with a modular design on each RSL. Third, the reshaping process is heterogeneous between the spatial and temporal dimensions, with the temporal dimension supporting connections both between adjacent layers or non-adjacent layers. These flexible connections provides a larger optimization space for the offline mapping than Fig. 4(c). Forth, the online and offline passes are further bridged by posing a FlexLattice IR, which guides the low-level operations by its translation to an instruction set. For general programs, the compilation flow can be summarized as follows.

1. Before program execution begins, an offline pass maps the program graph state to an efficient FlexLattice IR program, which translates to low-level instructions to guide real-time operations (Section 6).
2. During real-time execution, fusions between resource states are performed concurrently in a predetermined pattern that allows pipelined feed-forwards to improve the long-range-connectivity of the resulting graph state (Section 4).
3. The resulting random physical graph state is then reshaped to a 3D structure to fulfill the requirement of the IR program, with measurements performed on qubits according to the IR program (Section 5).

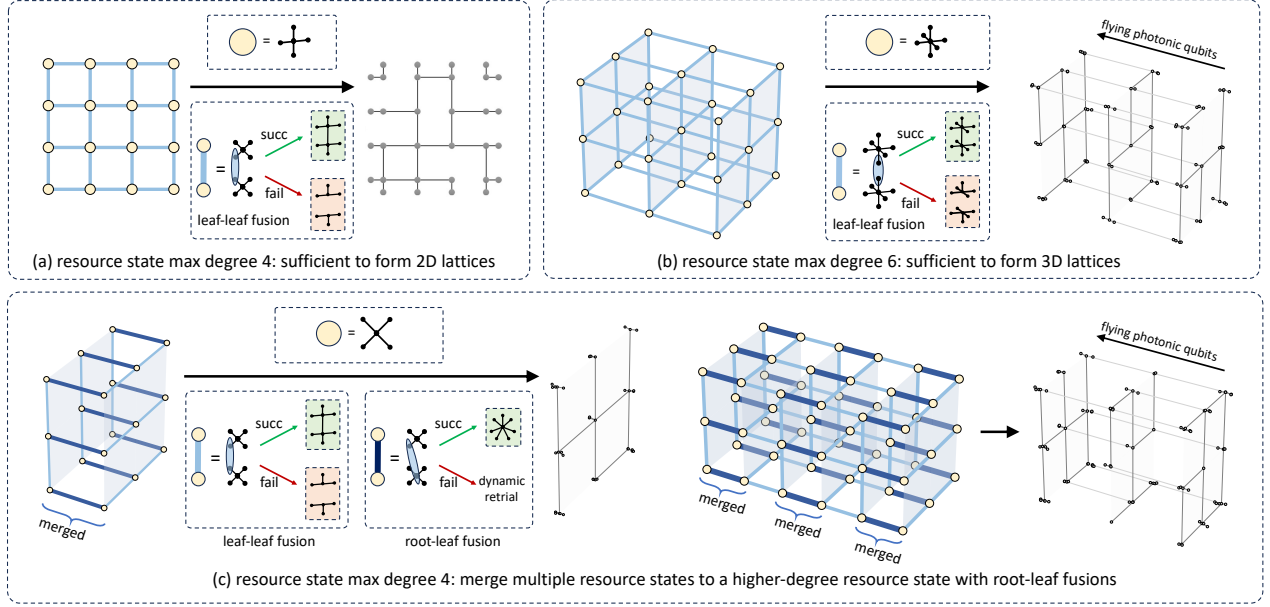


Figure 5. Fuse small resource states into 3D lattices.

## 4 Resource State Fusion

From the motivating example, it becomes evident that a dynamic adjustment of the fusion strategy among resource states lacks real-time scalability, as its prolonged decision making time could easily exceed the photon lifetime. To address this, we opt for a semi-static fusion strategy that generates program-agnostic physical graph states. This strategy is static in that it is predetermined independent of high-level programs, yet semi-static in that it allows pipelined feed-forward which induces only a constant overhead.

### 4.1 Sufficient / Insufficient Degree

The predetermined strategy attempts to create a lattice structure from the resource states, which is straightforward when resource states have sufficient node degrees, i.e., the maximum degree in the resource states surpasses that in the lattice. Fig. 5(a) shows the strategy of forming a 2D square lattice using 4-degree resource states. On the left side, each light blue line denotes a leaf-leaf fusion (degree=1) of the resource states (yellow circles). The right side displays the resulting random graph state due to fusion failures, with the consequences of successful and failed fusions depicted in the middle box. Similarly, Fig. 5(b) demonstrates the case of forming a cubic lattice 6-degree resource states. As resource states on realistic hardware may lack sufficient degrees [7], such as forming 3D cubic lattices using 4-degree resource states, we can increase resource state degrees by merging multiple RSLs into one layer using root-leaf fusions between resource states, represented by the dark blue lines in Fig. 5(c). Upon fusion success, a root-leaf fusion between two 4-degree resource states can generate a 7-degree resource state.

### 4.2 Removal of Irregular Structures

However, a failed root-leaf fusion may result in irregular cyclic structures in the generated graph state, leading to significant challenges for subsequent reshaping process. For example, a root-leaf fusion between two resource states  $A_0$  and  $B_0$  in Fig. 6 will generate a tree-like resource states  $A$  and a fully-connected cyclic  $B$ , which may result in complex structures if other qubits in  $B_0$  were fused with other resource states. To remove these cyclic structures, we will show that resource state  $B$  can be transformed to its local complementation, i.e., a tree-like resource state  $C$  by adjusting the bases of subsequent measurements and fusions. The operators for local complementation can therefore be propagated to the end of the computing process, and eventually can be removed by a re-interpretation of the final outcomes.

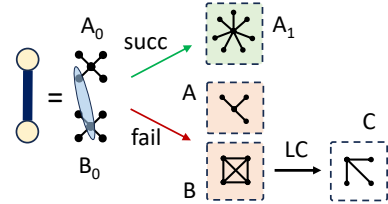


Figure 6. Root-leaf fusion failure.

**Definition 4.1** (local complementation). Letting  $G = (V, E)$  be a graph and  $v \in V$ , the local complement of  $G$  at  $v$ , denoted by  $\tau_v(G)$ , is obtained by complementing (inverting) the edges in the subgraph of  $G$  induced by the neighborhood  $N_v$  of  $v$  and leaving the rest of the graph unchanged.

**Proposition 4.2** ([39] LC-rule). *A graph state  $G$  can be transformed to its local complementation  $\tau_v(G)$  by applying the following sequence of single-qubit Clifford operations*

$$U_v(G) = \exp(-i\frac{\pi}{4}X_v) \prod_{u \in N_v} \exp(i\frac{\pi}{4}Z_u)$$

where  $N_v$  is the set of neighbors of  $v$  in  $G$ .

**Theorem 4.3.** *The operators  $U_Z^\pm = \exp(\pm i\frac{\pi}{4}Z)$  and  $U_X^\pm = \exp(\pm i\frac{\pi}{4}X)$  can both be propagated through a single-qubit equatorial measurement on the Bloch sphere, i.e., a measurement in the basis of  $\cos \phi X + \sin \phi Y$  where  $\phi \in [0, 2\pi)$ , as well as a  $Z$ -measurement by a change of measurement basis.*

*Proof.* A measurement of  $A$  on a single-qubit state  $|\psi\rangle$  collapses it to a state  $|\psi'\rangle \equiv M_{[A]}|\psi\rangle = \frac{I \pm A}{2}|\psi\rangle$  when the outcome is 0 and 1, respectively. It can then be verified that

$$\begin{aligned} M_{[\cos \phi X + \sin \phi Y]} U_Z^\pm &= U_Z^\pm M_{[\pm(\cos \phi Y - \sin \phi X)]} \\ M_{[\cos \phi X + \sin \phi Y]} U_X^\pm &= U_X^\pm M_{[\cos \phi X \pm \sin \phi Z]} \\ M_Z U_Z^\pm &= U_Z^\pm M_Z \\ M_Z U_X^\pm &= U_X^\pm M_Y \quad \square \end{aligned}$$

**Theorem 4.4.** *The operators  $U_Z^\pm = \exp(\pm i\frac{\pi}{4}Z)$  and  $U_X^\pm = \exp(\pm i\frac{\pi}{4}X)$  can both be propagated through a two-qubit  $XZ, ZX$  fusion, i.e., a joint measurement of  $X_1 Z_2, Z_1 X_2$  on qubit 1 and qubit 2, by a change of fusion basis. In particular, given a two-qubit quantum state  $|\psi\rangle$ ,*

*Proof.* A measurement of  $A$  on a two-qubit state  $|\psi\rangle$  collapses it to a state  $|\psi'\rangle \equiv M_{[A_1 A_2]}|\psi\rangle = \frac{I \pm A_1 A_2}{2}|\psi\rangle$  when the outcome is 0 and 1, respectively. It can then be verified that

$$\begin{aligned} M_{[X_1 Z_2]} M_{[Z_1 X_2]} U_{Z_1}^{\pm 1} U_{Z_2}^{\pm 2} &= U_{Z_1}^{\pm 1} U_{Z_2}^{\pm 2} M_{[\pm 1 Y_1 Z_2]} M_{[\pm 2 Z_1 Y_2]} \\ M_{[X_1 Z_2]} M_{[Z_1 X_2]} U_{X_1}^{\pm 1} U_{X_2}^{\pm 2} &= U_{X_1}^{\pm 1} U_{X_2}^{\pm 2} M_{[\pm 1 Y_1 X_2]} M_{[\pm 2 X_1 Y_2]} \\ M_{[X_1 Z_2]} M_{[Z_1 X_2]} U_{Z_1}^{\pm 1} U_{X_2}^{\pm 2} &= U_{Z_1}^{\pm 1} U_{X_2}^{\pm 2} M_{[\pm 1 \mp 2 Y_1 Y_2]} M_{[Z_1 X_2]} \quad \square \end{aligned}$$

### 4.3 Pipelined Feed-forward

Despite being predetermined, the semi-static fusion strategy allows collective feed-forwards which can be pipelined to reduce the overhead. On one hand, this is because the propagation of operators for local complementation requires an adaptive adjustment of measurement and fusion bases. On the other hand, the connectivity of the generated random graph state can be enhanced by mitigating the fusion failures, including retrying failed leaf-leaf fusions with redundant degrees (e.g., the 7<sup>th</sup> degree of  $A_1$  in Fig. 6) and retrying failed root-leaf fusions with remaining degrees (e.g.,  $A$  and  $C$  in Fig. 6). These feed-forwards can be pipelined as they involve only one or few consecutive RSLs. For example, the second feed-forward round of a (merged) RSL can be conducted concurrently with the first round of the next one, thereby introducing only a constant overhead for the overall program execution.

## 5 Random State Reshaping

Similar to the impracticality of dynamically adjusting fusion strategies, dynamically mapping program graph states onto the random physical graph states demands computational complexity exceeding the photon lifetime. To address this, we reshape each RSL to a program-agnostic 2D lattice structure and preserve flexibility for the connections among them. This (2+1)-D design, motivated by the continuous generation of RSLs over time and the presence of delay lines, aims to minimize the dynamic feed-forward while providing enough room for program optimization.

### 5.1 Efficient 2D Renormalization

On each (merged) RSL, we apply a process known as renormalization, which reshapes the largest connected component of the random physical graph state to a coarse-grained 2D lattice. The key to its viability lies in the percolation phenomenon [23–25]. That is, when the fusion success (or edge connectivity) probability exceeds a certain threshold, the random physical graph state undergoes a phase transition from short-range connectivity to long-range connectivity, leading to the largest connected component reaching a comparable size with the original graph state. Since fusions on each RSL are constrained as a squared lattice, the percolation threshold is only 0.5 [40], lower than the practical fusion success probability.

Identifying intersections of horizontal and vertical paths within this component reveals a coarse-grained square lattice, represented by bold nodes and edges in Fig. 7(b). Specifically, we search for vertical paths from left to right and horizontal paths from bottom to top, enforcing distinct vertical or horizontal paths to maintain a minimum separation of at least one qubit. For each vertical (horizontal) path, a connectivity check is conducted between nodes at the top (left) and bottom (right), facilitated by a disjoint-set data structure to reduce the complexity. Upon confirming connectivity, a breadth-first search (BFS) is applied to determine the shortest path, ensuring it remains free of self-tangling. To further prevent tangling between vertical and horizontal paths, we remove the surrounding qubits of each identified path after discovery, preventing their interference with subsequent searches. Considering the removals, an alternating search of vertical and horizontal paths emerges as an effectively searching order.

To improve real-time scalability, the 2D renormalization is designed to allow **modularity**, with areas on the RSL renormalized concurrently and then joined together. As shown in Fig. 8, the RSL is divided into several modules of size  $L_{Module} \times L_{Module}$ , with some intervals of length  $L_{Interval}$  left in between for joining the modules with connected paths. This modularity leads to a time complexity of  $O(1)$  constrained by the size of modules, with the complexity within each module further reduced by employing a disjoint-set data

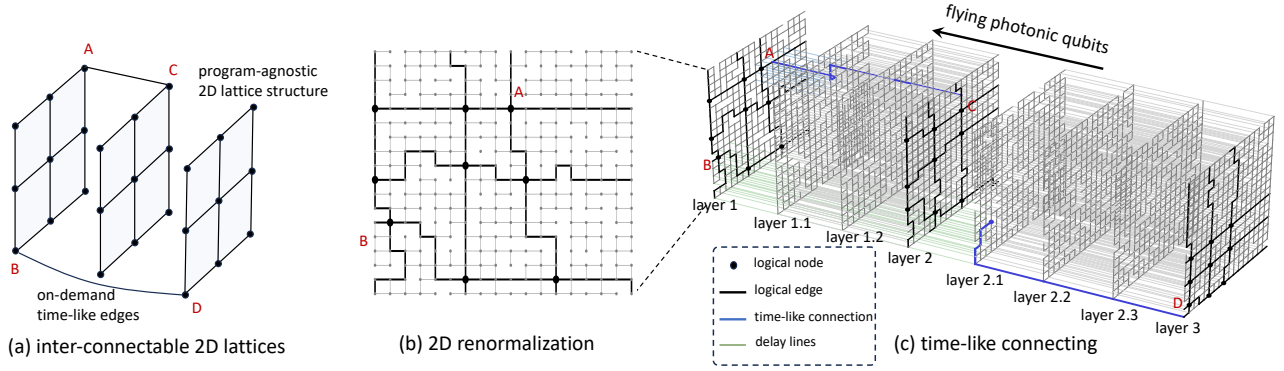


**Figure 7.** (2+1)-D renormalization for handling random graph states generated by fusions.

structure. However, it also introduces a resource overhead due to the presence of intervals and the possible missing connected paths between the modules. A suitable ratio of  $L_{Module}$  and  $L_{Interval}$ , defined as *MI ratio*, can help mitigate this resource overhead, as will be demonstrated Section 7.

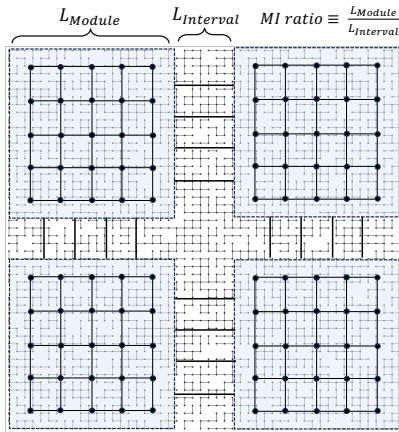


**Figure 8.** Modular renormalization.

## 5.2 Flexible Time-like Connection

Nodes on the renormalized 2D lattices can be connected along the third dimension of time, referred to as *time-like connections*. These connections can be established both between adjacent 2D lattices or across non-adjacent 2D lattices, which are called *adjacent-layer connections* and *cross-layer connections*. The connections to establish are given by the IR program at the beginning of execution, leading to a 3D graph consisting of interconnected 2D layers as illustrated in Fig. 7(a). The process of generating this 3D graph is illustrated in Fig. 7(c) on 8 RSLs, with the adjacent-layer connection  $AC$  and the cross-layer connection  $BD$  being implemented through the bold purple paths.

In particular, this process involves an attempt of 2D renormalization on each RSL. The successful ones then serves as

a *logical layer*, which are indexed with integers in Fig. 7(c), while the failed ones serve as *routing layers*, which are indexed with decimals in Fig. 7(c). The renormalization on an RSL is considered successful if:

1. The renormalized 2D lattice reaches a size of choice, equivalent with a choice of average node size, where

$$\text{average\_node\_size} = \frac{\text{RSL\_size}}{\text{renormalized\_lattice\_size}}$$

2. The RSL can establish necessary time-like connections with prior logical layers.

To establish a time-like connection between two nodes, a set of qubits around the earlier node are fused with corresponding qubits on a correct subsequent layer. For adjacent-layer connection such as  $AC$ , the set of qubits around  $A$  are directly fused to the next layer, which is layer 1.1 in Fig. 7(c). For cross-layer connection such as  $BD$ , the set of qubits around  $B$  are temporarily stored in delay lines as represented by the green thin lines in Fig. 7(c), until they can be fused to layer 2.1, which is the first RSL between the layer of the other node  $D$  (layer 3) and its prior logical layer (layer 2). In contrast, all qubits of every path routing layers are directly fused with their next layer, as depicted by the grey thin lines in Fig. 7(c).

Subsequently, a path searching between the two nodes is conducted within the random physical graph state, exemplified by the bold purple lines  $AC$  and  $BD$  in Fig. 7(c). Again, this is achieved by a connectivity check utilizing a disjoint-set data structure and a BFS for the shortest path. If the connectivity check yields a negative result, it indicates that the current RSL fails to meet the second condition, thus the RSL would serve as a routing layer. It is worth mentioning that this process can tolerate the photon loss by treating a fusion as successful only if both the input photons are detected. Effectively, the presence of photon loss causes a reduction of the fusion success probability, possibly leading to more path routing layers between logical layers.

## 6 IR for Offline Optimization

The structures supported by the reshaping of the random physical graph state motivates a new IR, which maintains the high-level program information and allows sophisticated offline optimizations. Specifically, an offline mapping algorithm can be employed to transform the program graph state to an IR graph state. This IR will then guide the real-time operations through a low-level instruction set.

### 6.1 FlexLattice IR

The reshaped physical graph state enables the abstraction of a deterministic virtual hardware, characterized by 2D layers in a lattice structure that are flexibly interconnectable in the third dimension, as depicted in Fig. 9(b). This virtual hardware allows for the embedding of a family of graphs sharing similar features as demonstrated in Fig. 9(c), motivating the introduction of a *FlexLattice* IR. The purpose of this IR is to preserve the high-level program information while providing a maximal optimization space supported by the hardware. The rationale for this IR is supported by the fact that any program graph state can be transformed into such a representation, as illustrated in Fig. 9(a)→(c)→(d).

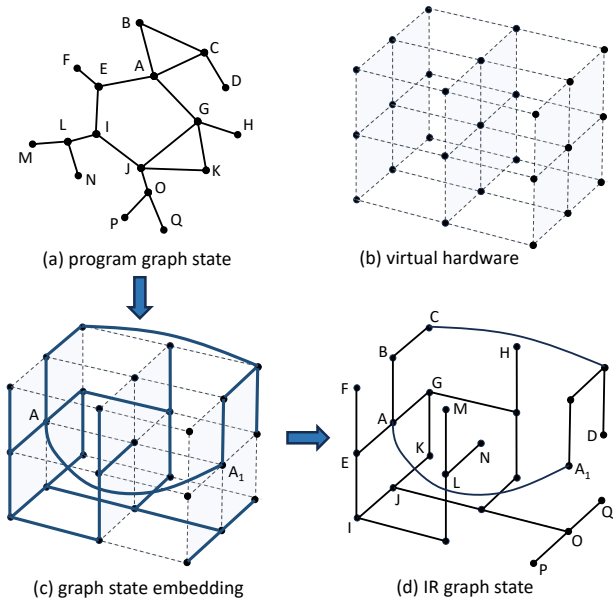


**Figure 9.** Offline Mapping onto the virtual hardware.

Specifically, a FlexLattice graph is defined by the following features.

1. The graph has a  $(2+1)$ -D structure, with each 2D layer being a subgraph of a lattice with a fixed size.
2. Edges on the third dimension connect nodes at the same positions across different 2D lattice layers, irrespective of whether these layers are adjacent or not.

3. Each node has at most two edges in the third dimension, i.e., at most one with nodes on preceding layers and at most one with those on subsequent layers.

### 6.2 Instruction Set

An IR graph state can be implemented on the virtual hardware by a low-level instruction set defined as below, with nodes in the high-level program graph state represented by `g_node` and nodes on the virtual hardware represented by `v_node`. If not adjusted by the low-level instructions, qubits in the physical graph state are subject to  $Z$ -measurements by default. A virtual node can be mapped to a `g_node` or used as an ancilla node for routing. In the former case the corresponding qubit will be measured according to the measurement pattern, while in the latter case it will be measured in  $X$ - or  $Y$ -basis adaptively. A virtual node can also be stored into or retrieved from a virtual cache by pushing or popping its surrounding qubits to or from the delay lines. Spatial edges between adjacent nodes on the same layer can be enabled by setting associated qubits to  $X$ - or  $Y$ -measurements, while temporal edges between nodes at the same position of adjacent layers can be enabled by establishing an adjacent-layer time-like connection.

```
map_v_node(v_node, g_node)
make_v_node_ancilla(v_node)
store_v_node(v_node)
retrieve_v_node(v_node, position)
enable_spatial_v_edge(v_node, adjacent_v_node)
enable_temporal_v_edge(v_node, adjacent_v_node)
```

Cross-layer time-like connections between layer  $m$  and layer  $n$  ( $> m$ ) can be established by a combination of three instructions, i.e., storing the node at layer  $m$  into the virtual cache, retrieve it at layer  $n - 1$ , and enable a temporal edge between layer  $n - 1$  and layer  $n$ . For example, the cross-layer temporal edge between ancilla node  $A$  at  $(1,1,0)$  and graph node  $A_1$   $(1,1,2)$  in Fig. 9(d) can be implemented with the instructions below. Note that retrieving `v_node` at layer  $n - 1$  does not conflict with the original `v_node` at layer  $n - 1$ . This is because the original node at layer  $n - 1$  would not have an edge with layer  $n$ , since each node in a FlexLattice graph has at most one edge with preceding layers. This implies that the original node will either have no further edges or will be stored in the virtual cache at layer  $n - 1$ .

```
map_v_node((1, 1, 0), A)
store_v_node((1, 1, 0))
...
retrieve_v_node((1, 1, 0), (1, 1, 1))
make_v_node_ancilla((1, 1, 2))
enable_temporal_v_edge((1, 1, 1), (1, 1, 2))
```

### 6.3 Offline Mapping

With this IR, graph state mapping algorithms such as that in OneQ can be utilized as an offline pass to produce an efficient IR program. To support large-scale programs, we extend OneQ’s mapping algorithm with two further optimizations. First, to reserve enough space for routing and avoid node congestion, we limit the percentage of incomplete nodes on each layer within a certain threshold, with incomplete nodes defined as those mapped nodes whose edges are not all mapped yet. Second, to mitigate the increasing demand on classical memory for graph information storage, we employ a refresh mechanism, which periodically retrieves all nodes stored in the virtual cache, refreshing them by connecting them with current one or multiple layers, and storing them again.

## 7 Evaluation

### 7.1 Experiment Setup

**Baseline.** We compare the performance of our framework with the efficient photonic MBQC compiler OneQ. Since OneQ is not able to handle fusion failures, we employ it with a repeat-until-success strategy. Specifically, for each RSL we conduct the fusions implied by OneQ repeatedly until all fusions are successful. Subsequently, the successful RSL is fused with its preceding RSLs. If failures occur in the inter-RSL fusions, the entire compilation is reset and repeated until success.

**Metrics.** Aligning with OneQ, we evaluate the performance of compilation with two metrics: the number of consumed RSL, denoted by #RSL, and the number of required fusions, denoted by #fusion. In particular, a smaller #RSL indicates less execution time of the program and less chance for photon loss, while a smaller #fusion implies less operations and less chance for error occurrence.

**Table 1.** Benchmark Programs.

Fusion Success Rate	#Qubits	Virtual Hardware Size	RSL Size
0.90	4	2x2	24x24
	9	3x3	36x36
	25	5x5	60x60
0.75	4	2x2	48x48
	25	5x5	120x120
	64	8x8	192x192

**Photonic Hardware Model.** We adopt the same photonic hardware architecture with OneQ, as introduced in Section 2. In the main experiment, the comparison with OneQ is performed with 4-qubit star-like resource states, and the sizes of hardware for different benchmarks are listed in Table 1. Subsequent experiments for further analysis are conducted with 7-qubit star-like resource states, which naturally have sufficient degrees for forming 3D lattice-like graph states.

**Benchmark programs.** We select a set of benchmark programs including Quantum Approximate Optimization Algorithm (QAOA), Quantum Fourier transform (QFT), Ripple-Carry Adder (RCA) [41] and Variational Quantum Eigensolver (VQE). For QAOA, we choose the graph maxcut problem on randomly generated graphs. Specifically, the graphs are generated by randomly connecting half of all its possible edges. For VQE, we follow the commonly used full-entanglement ansatz, which proves to be an expressive ansatz [42, 43]. In table 1, we list the benchmarks with their numbers of qubits in the circuit representation. We also list the sizes of virtual hardware layers, along with the required sizes of RSLs to construct them.

### 7.2 Experiment Result

In this subsection, we firstly show the performance of our compiler in comparison with OneQ. Then we analyze the effects of underlying resource states, hardware size and fusion success probability, for which we only focus on #RSL. This is because unlike OneQ, the #fusion in OnePerc is predictable from its #RSL, thus following a same trend with #RSL.

**Performance.** Table 2 presents the comparison of our framework with OneQ. The results indicate a significant reduction of #RSL and #fusion by our framework. Specifically, the results show that OneQ can work only in the region of small programs and high fusion success probabilities. When the fusion success probability decreases to a practical value around 0.75, it takes more than  $10^6$  RSLs even for executing the 4-qubit benchmarks. This implies OneQ’s non-scalability due to its lack of capability in systematically handling the randomness of fusion failure. In contrast, our framework can work well with a practical success probability, demonstrating an increasing outperformance over OneQ as the programs scale up.

**Resource State Size.** Our compiler has a general applicability to the underlying resource states of various sizes. Fig. 10(a) illustrates the varying #RSL when executing the programs with star-like resource states of different sizes, i.e., consisting of different numbers of qubits. It can be seen that the #RSL decreases as the size of resource states increases. This is because a larger resource state can participate in fusions with more qubit degrees, without the need of increasing the degrees by merging multiple RSLs.

**Hardware Size.** Our compiler has an adaptability to various hardware sizes. Fig. 10(b) shows the varying #RSL when executing the programs on photonic hardware of different sizes, i.e., with different sizes of RSLs. It can be seen that a larger photonic hardware leads to a reduced #RSL, which indicates that our framework can effectively utilize the computing resource as it scales up. In particular, a larger RSL can enable a larger renormalized lattice, thus a larger virtual hardware. This provides the offline mapping with an

**Table 2.** The results of OnePerc and its relative performance to the baseline.

Fusion Success Rate	Benchmark Name	OneQ #RSL	OnePerc #RSL	#RSL Improv.	OneQ #Fusion	OnePerc #Fusion	#Fusion Improv.
0.90 (hyper-advanced)	QAOA-4	304	84	3.62	13,990	117,664	0.12
	QFT-4	3,759	174	21.59	180,634	274,155	0.66
	RCA-4	3,107	237	13.11	63,814	373,646	0.17
	VQE-4	56	22	2.55	1,707	33,526	0.05
	QAOA-9	> 10 <sup>6</sup>	240	> 10 <sup>3</sup>	> 10 <sup>10</sup>	855,354	> 10 <sup>4</sup>
	QFT-9	> 10 <sup>6</sup>	570	> 10 <sup>3</sup>	> 10 <sup>10</sup>	2,031,813	> 10 <sup>3</sup>
	RCA-9	> 10 <sup>6</sup>	1,017	> 10 <sup>2</sup>	> 10 <sup>10</sup>	3,627,950	> 10 <sup>3</sup>
	VQE-9	> 10 <sup>6</sup>	156	> 10 <sup>3</sup>	> 10 <sup>10</sup>	555,065	> 10 <sup>4</sup>
	QAOA-25	> 10 <sup>6</sup>	768	> 10 <sup>3</sup>	> 10 <sup>10</sup>	7,637,711	> 10 <sup>3</sup>
	QFT-25	> 10 <sup>6</sup>	2,418	> 10 <sup>2</sup>	> 10 <sup>10</sup>	24,065,102	> 10 <sup>2</sup>
RCA-25	> 10 <sup>6</sup>	3,111	> 10 <sup>2</sup>	> 10 <sup>10</sup>	30,962,172	> 10 <sup>2</sup>	
VQE-25	> 10 <sup>6</sup>	705	> 10 <sup>3</sup>	> 10 <sup>10</sup>	7,010,656	> 10 <sup>3</sup>	
0.75 (practical)	QAOA-4	1,708	48	35.58	119,731	169,431	0.71
	QFT-4	> 10 <sup>6</sup>	210	> 10 <sup>3</sup>	> 10 <sup>10</sup>	746,977	> 10 <sup>4</sup>
	RCA-4	> 10 <sup>6</sup>	201	> 10 <sup>3</sup>	> 10 <sup>10</sup>	714,835	> 10 <sup>4</sup>
	VQE-4	1,017	23	44.22	25,354	96,332	0.26
	QAOA-25	> 10 <sup>6</sup>	705	> 10 <sup>3</sup>	> 10 <sup>10</sup>	15,781,250	> 10
	QFT-25	> 10 <sup>6</sup>	2,271	> 10 <sup>2</sup>	> 10 <sup>10</sup>	50,835,771	> 10
	RCA-25	> 10 <sup>6</sup>	3,252	> 10 <sup>2</sup>	> 10 <sup>10</sup>	72,795,212	> 10
	VQE-25	> 10 <sup>6</sup>	759	> 10 <sup>3</sup>	> 10 <sup>10</sup>	17,292,345	> 10
	QAOA-64	> 10 <sup>6</sup>	2,787	> 10 <sup>2</sup>	> 10 <sup>10</sup>	62,386,302	> 10
	QFT-64	> 10 <sup>6</sup>	9,609	> 10 <sup>2</sup>	> 10 <sup>10</sup>	215,095,078	> 10
RCA-64	> 10 <sup>6</sup>	8,001	> 10 <sup>2</sup>	> 10 <sup>10</sup>	179,100,397	> 10	
VQE-64	> 10 <sup>6</sup>	3,132	> 10 <sup>2</sup>	> 10 <sup>10</sup>	70,109,041	> 10	

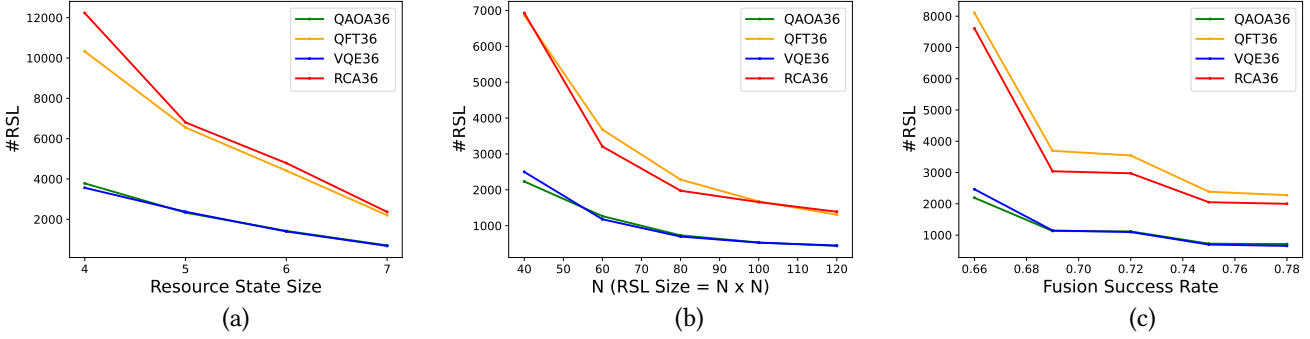


**Figure 10.** Effects of resource state size (a), hardware size (b) and fusion success probability (c), with the resource states being 7-qubit ones for (b)(c), hardware size being 84x84 for (a)(c), and the fusion success probability being 0.75 for (a)(b).

increased space for flexible routing, thereby reducing the required logical layer and, consequently, the #RSL.

**Fusion Success Probability.** Our compiler has a capability of tolerating fusion failures at a practical level. Fig. 10(c) shows the varying #RSL when executing programs under different fusion success probabilities. It can be seen that our compiler can tolerate a fusion success probability as low as 0.66, with the #RSL decreasing with a higher fusion success probability. This is because a higher fusion success probability results in a larger renormalized lattice on RSLs, enabling a larger virtual hardware. This provides the offline mapping with an increased space for flexible routing, thereby reducing the required logical layer and, consequently, the #RSL.

### 7.3 Scalability and Parallelism

**Scalability.** Our compiler presents a great scalability, characterized by the stable overhead as the computing scales up. Fig. 11(a) shows the average node size of 2D renormalization as the hardware size increases. In particular, it keeps stable against the hardware size, being smaller with a higher fusion success probability. Fig. 11(b) shows the average ratio of RSL to logical layers as the program size increases. In particular, it first increases with the program size then soon gets stable at around 3, implying the successful formation of a logical layer about every 3 RSLs. These stabilities provide a predictability of the resource consumption and ensures the scalability of our framework.

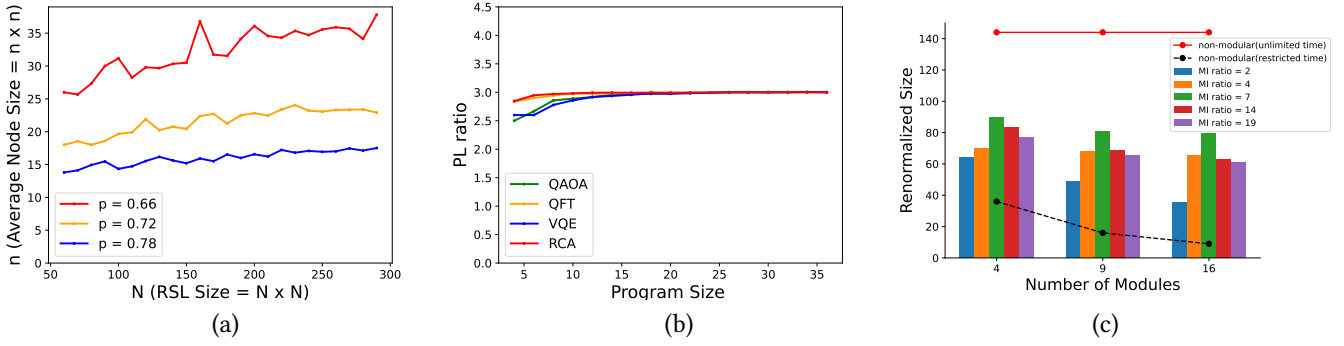


**Figure 11.** Scalability and parallelism of OnePerc with 7-qubit resource states, with fusion success probability being 0.75 for (b)(c), average node size chosen as  $20 \times 20$  for (b)(c), hardware size being  $100 \times 100$  for (b) and  $240 \times 240$  for (c).

**Parallelism.** While our framework achieves a notable real-time scalability with a modular 2D renormalization, it involves a tradeoff between the parallelism and the resource efficiency. This is because the presence of intervals between the modules reduces the available resource on each RSL (Fig. 8). To evaluate this resource overhead, Fig. 11(c) depicts the size of the renormalized 2D lattice against the number of modules. For comparison, the red dots represent the renormalized lattice size of a non-modular algorithm in an unlimited time, while the black dots represent the renormalization size of the non-modular algorithm in a time restricted by that consumed by the modular approach.

It can be seen that the renormalized lattice by the modular approach is around 60% of that by the non-modular approach with unlimited time, which decreases slightly with the number of modules. This is because an increased number of modules leads to a higher probability of being unable to connect the corresponding paths across different modules. However, the renormalized lattice is significantly larger than that can be achieved by the non-modular in the restricted time, which ranges from  $2\times$  to  $7\times$  as the number of modules increases from 4 to 16. This is very important since the time for the online algorithm is always restricted by the limited lifetime of photons. Overall, Fig. 11(c) indicates that our framework can significantly improve the real-time scalability with a relatively stable overhead of computing resource.

#### 7.4 Hyper Parameters

**MI Ratio.** The size of renormalized lattices also relies on a suitable choice of MI ratio (defined in Fig. 8). Fig. 11(c) illustrates the renormalized lattice size with different choices of MI ratios. It can be seen that the renormalization size first increases with the MI ratio and then decreases, peaking at around 7 regardless of the number of modules. This is because an excessively low MI ratio leads to a waste of resource with its wide interval space while an overly high MI ratio increases the probability of unable to connect corresponding paths with its restricted routing space in the intervals.

**Average Stripe Size.** A suitable choice of average node size is important for reshaping, as it determines the target size of a successful 2D lattice. Fig. 12 illustrates the success probability of reaching different predetermined lattice sizes, i.e., different choices of average node size. It can be seen that the success probability approaches 1 rapidly as the target lattice becomes more coarse-grained. This sharp transition motivates us to choose the smallest average node size that brings the success probability close to 1.

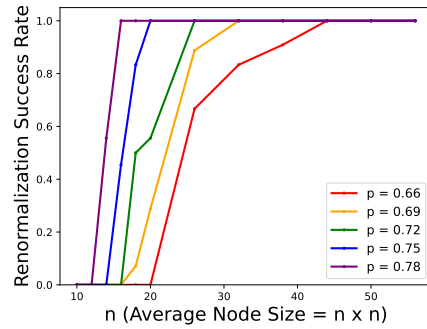


**Figure 12.** Effect of choices of average node size.

## 8 Conclusion

In this work, we provide in-depth analysis and discussion of the challenges for photonic quantum compilation brought by the probabilistic operations involved in the computing. We propose a randomness-aware compiler to handle these probabilistic operations, demonstrating a concurrent achievement of scalability and efficiency on photonic systems. With this being said, we believe that there is still significant potential for fully exploring the entire optimization space. We hope that our work could attract more effort from the computer architecture and compiler community to explore the advantages of photonic quantum computing and overcome the unique challenges.

## References

- [1] Jeremy L. O'Brien, Akira Furusawa, and Jelena Vučković. Photonic quantum technologies. *Nature Photonics*, 3(12):687, 2009. URL: <https://www.nature.com/articles/nphoton.2009.229>, doi:10.1038/nphoton.2009.229.
- [2] S. Bogdanov, M. Y. Shalaginov, A. Boltasseva, and V. M. Shalaev. Material platforms for integrated quantum photonics. *Opt. Mater. Express*, 7(1):111–132, Jan 2017. URL: <http://opg.optica.org/ome/abstract.cfm?URI=ome-7-1-111>, doi:10.1364/OME.7.000111.
- [3] Han-Sen Zhong, Hui Wang, Yu-Hao Deng, Ming-Cheng Chen, Li-Chao Peng, Yi-Han Luo, Jian Qin, Dian Wu, Xing Ding, Yi Hu, Peng Hu, Xiao-Yan Yang, Wei-Jun Zhang, Hao Li, Yuxuan Li, Xiao Jiang, Lin Gan, Guangwen Yang, Lixing You, Zhen Wang, Li Li, Nai-Le Liu, Chao-Yang Lu, and Jian-Wei Pan. Quantum computational advantage using photons. *Science*, 370(6523):1460–1463, 2020. URL: <https://www.science.org/doi/10.1126/science.abe8770>, doi:10.1126/science.abe8770.
- [4] Han-Sen Zhong, Yu-Hao Deng, Jian Qin, Hui Wang, Ming-Cheng Chen, Li-Chao Peng, Yi-Han Luo, Dian Wu, Si-Qiu Gong, Hao Su, Yi Hu, Peng Hu, Xiao-Yan Yang, Wei-Jun Zhang, Hao Li, Yuxuan Li, Xiao Jiang, Lin Gan, Guangwen Yang, Lixing You, Zhen Wang, Li Li, Nai-Le Liu, Jelmer J. Renema, Chao-Yang Lu, and Jian-Wei Pan. Phase-programmable gaussian boson sampling using stimulated squeezed light. *Phys. Rev. Lett.*, 127:180502, Oct 2021. URL: <https://link.aps.org/doi/10.1103/PhysRevLett.127.180502>, doi:10.1103/PhysRevLett.127.180502.
- [5] Lars S. Madsen, Fabian Laudenbach, Mohsen Falamarzi, Askarani, Fabien Rortais, Trevor Vincent, Jacob F. F. Bulmer, Filippo M. Miatto, Leonhard Neuhaus, Lukas G. Helt, Matthew J. Collins, Adriana E. Lita, Thomas Gerrits, Sae Woo Nam, Varun D. Vaidya, Matteo Menotti, Ish Dhand, Zachary Vernon, Nicolás Quesada, and Jonathan Lavoie. Quantum computational advantage with a programmable photonic processor. *Nature*, 606(7912):75–81, Jun 2022. URL: <https://www.nature.com/articles/s41586-022-04725-x>, doi:10.1038/s41586-022-04725-x.
- [6] JM Arrazola, V Bergholm, K Brádler, TR Bromley, MJ Collins, I Dhand, A Fumagalli, T Gerrits, A Goussev, LG Helt, et al. Quantum circuits with many photons on a programmable nanophotonic chip. *Nature*, 591(7848):54–60, 2021. URL: <https://www.nature.com/articles/s41586-021-03202-1>, doi:10.1038/s41586-021-03202-1.
- [7] Terry Rudolph. Fusion based photonic quantum computing. In *APS March Meeting Abstracts*, volume 2022, pages D28–001, 2022. URL: <https://www.nature.com/articles/s41467-023-36493-1>, doi:10.1038/s41467-023-36493-1.
- [8] Michel H Devoret and Robert J Schoelkopf. Superconducting circuits for quantum information: an outlook. *Science*, 339(6124):1169–1174, 2013. URL: <https://science.org/doi/10.1126/science.1231930>, doi:10.1126/science.1231930.
- [9] Colin D Bruzewicz, John Chiaverini, Robert McConnell, and Jeremy M Sage. Trapped-ion quantum computing: Progress and challenges. *Applied Physics Reviews*, 6(2):021314, 2019. URL: <https://pubs.aip.org/aip/apr/article-abstract/6/2/021314/570103/Trapped-ion-quantum-computing-Progress-and?redirectedFrom=fulltext>, doi:10.1063/1.5088164.
- [10] Mark Saffman. Quantum computing with atomic qubits and rydberg interactions: progress and challenges. *Journal of Physics B: Atomic, Molecular and Optical Physics*, 49(20):202001, 2016. URL: <https://iopscience.iop.org/article/10.1088/0953-4075/49/20/202001>, doi:10.1088/0953-4075/49/20/202001.
- [11] Fabian Ewert and Peter van Loock. 3/4-efficient bell measurement with passive linear optics and unentangled ancillae. *Physical review letters*, 113(14):140403, 2014. URL: <https://journals.aps.org/prl/abstract/10.1103/PhysRevLett.113.140403>, doi:10.1103/PhysRevLett.113.140403.
- [12] Warren P Grice. Arbitrarily complete bell-state measurement using only linear optical elements. *Physical Review A*, 84(4):042331, 2011. URL: <https://journals.aps.org/prl/abstract/10.1103/PhysRevA.84.042331>, doi:10.1103/PhysRevA.84.042331.
- [13] Michael A Nielsen and Isaac L Chuang. Quantum computation and quantum information. *Phys. Today*, 54(2):60, 2001. URL: [https://cds.cern.ch/record/465953/files/0521635039\\_TOC.pdf](https://cds.cern.ch/record/465953/files/0521635039_TOC.pdf).
- [14] Qiskit contributors. Qiskit: An open-source framework for quantum computing, 2023. URL: <https://zenodo.org/records/2562111>, doi:10.5281/zenodo.2573505.
- [15] Seyon Sivarajah, Silas Dilkes, Alexander Cowtan, Will Simmons, Alec Edgington, and Ross Duncan. t|ket>: A retargetable compiler for nisq devices. *Quantum Science and Technology*, 6, 04 2020. URL: <https://iopscience.iop.org/article/10.1088/2058-9565/ab8e92>, doi:10.1088/2058-9565/ab8e92.
- [16] Robert Raussendorf, Dan Browne, and Hans Briegel. Measurement-based quantum computation on cluster states. *Raussendorf, R. and Browne, D.E. and Briegel, H.J. (2003) Measurement-based quantum computation on cluster states. Physical Review A, 68 (2). 022312.1-022312.32. ISSN 10502947, 68, 08 2003.* URL: <https://journals.aps.org/prl/abstract/10.1103/PhysRevA.68.022312>, doi:10.1103/PhysRevA.68.022312.
- [17] Anne Broadbent and Elham Kashefi. Parallelizing quantum circuits. *Theoretical computer science*, 410(26):2489–2510, 2009. URL: <https://www.sciencedirect.com/science/article/pii/S0304397508009377?via%3Dihub>, doi:10.1016/j.tcs.2008.12.046.
- [18] Hezi Zhang, Anbang Wu, Yuke Wang, Gushu Li, Hassan Shapourian, Alireza Shabani, and Yufei Ding. Oneq: A compilation framework for photonic one-way quantum computation. In *Proceedings of the 50th Annual International Symposium on Computer Architecture*, pages 1–14, 2023. URL: <https://dl.acm.org/doi/10.1145/3579371.3589047>, doi:10.1145/3579371.3589047.
- [19] Ming-Jun Li and Tetsuya Hayashi. Advances in low-loss, large-area, and multicore fibers. In *Optical Fiber Telecommunications VII*, pages 3–50. Elsevier, 2020. URL: <https://www.sciencedirect.com/science/article/abs/pii/B9780128165027000014>, doi:10.1016/B978-0-12-816502-7.00001-4.
- [20] Pieter Kok, William J Munro, Kae Nemoto, Timothy C Ralph, Jonathan P Dowling, and Gerard J Milburn. Linear optical quantum computing with photonic qubits. *Reviews of modern physics*, 79(1):135, 2007. URL: <https://journals.aps.org/rmp/abstract/10.1103/RevModPhys.79.135>, doi:10.1103/RevModPhys.79.135.
- [21] Guilherme Luiz Zanin, Maxime J Jacquet, Michele Spagnolo, Peter Schiansky, Irati Alonso Calafell, Lee A Rozema, and Philip Walther. Fiber-compatible photonic feed-forward with 99% fidelity. *Optics Express*, 29(3):3425–3437, 2021. URL: <https://opg.optica.org/oe/fulltext.cfm?uri=oe-29-3-3425&id=446800>, doi:10.1364/OE.409867.
- [22] Atsushi Sakaguchi, Shunya Konno, Fumiya Hanamura, Warit Asavanant, Kan Takase, Hisashi Ogawa, Petr Marek, Radim Filip, Jun-ichi Yoshikawa, Elanor Huntington, et al. Nonlinear feedforward enabling quantum computation. *Nature Communications*, 14(1):3817, 2023. URL: <https://www.nature.com/articles/s41467-023-39195-w>, doi:10.1038/s41467-023-39195-w.
- [23] Mercedes Gimeno-Segovia, Pete Shadbolt, Dan E Browne, and Terry Rudolph. From three-photon ghz states to universal ballistic quantum computation. 2015. URL: <https://journals.aps.org/prl/abstract/10.1103/PhysRevLett.115.020502>, doi:10.1103/PhysRevLett.115.020502.
- [24] Mihir Pant, Don Towsley, Dirk Englund, and Saikat Guha. Percolation thresholds for photonic quantum computing. *Nature communications*, 10(1):1070, 2019. URL: <https://www.nature.com/articles/s41467-019-08948-x>, doi:10.48550/arXiv.1701.03775.

- [25] Daniel E Browne, Matthew B Elliott, Steven T Flammia, Seth T Merkel, Akimasa Miyake, and Anthony J Short. Phase transition of computational power in the resource states for one-way quantum computation. *New Journal of Physics*, 10(2):023010, 2008. URL: <https://iopscience.iop.org/article/10.1088/1367-2630/10/2/023010>, doi:10.1088/1367-2630/10/2/023010.
- [26] Sergei Slussarenko and Geoff J Pryde. Photonic quantum information processing: A concise review. *Applied Physics Reviews*, 6(4):041303, 2019. URL: <https://pubs.aip.org/aip/apr/article/6/4/041303/997349/Photonic-quantum-information-processing-A-concise>, doi:10.1063/1.5115814.
- [27] Philip Walther, Kevin J Resch, Terry Rudolph, Emmanuel Schenck, Harald Weinfurter, Vlatko Vedral, Markus Aspelmeyer, and Anton Zeilinger. Experimental one-way quantum computing. *Nature*, 434(7030):169–176, 2005. URL: <https://www.nature.com/articles/nature03347>, doi:10.1038/nature03347.
- [28] Giuseppe Vallone, Gaia Donati, Natalia Bruno, Andrea Chiuri, and Paolo Mataloni. Experimental realization of the deutsch-jozsa algorithm with a six-qubit cluster state. *Physical Review A*, 81(5):050302, 2010. URL: <https://journals.aps.org/pr/abstract/10.1103/PhysRevA.81.050302>, doi:10.1103/PhysRevA.81.050302.
- [29] Mark S Tame, Bryn A Bell, Carlo Di Franco, William J Wadsworth, and John G Rarity. Experimental realization of a one-way quantum computer algorithm solving simon’s problem. *Physical Review Letters*, 113(20):200501, 2014. URL: <https://journals.aps.org/prl/abstract/10.1103/PhysRevLett.113.200501>, doi:10.1103/PhysRevLett.113.200501.
- [30] Simone Ferrari, Carsten Schuck, and Wolfram Pernice. Waveguide-integrated superconducting nanowire single-photon detectors. *Nanophotonics*, 7(11):1725–1758, 2018. URL: <https://www.degruyter.com/document/doi/10.1515/nanoph-2018-0059/html?lang=en>, doi:10.1515/nanoph-2018-0059.
- [31] Jianwei Wang, Stefano Paesani, Yunhong Ding, Raffaele Santagati, Paul Skrzypczyk, Alexia Salavrakos, Jordi Tura, Remigiusz Augusiak, Laura Mančinska, Davide Bacco, et al. Multidimensional quantum entanglement with large-scale integrated optics. *Science*, 360(6386):285–291, 2018. URL: <https://www.science.org/doi/10.1126/science.aar7053>, doi:10.1126/science.aar7053.
- [32] Vinicius S Ferreira, Gihwan Kim, Andreas Butler, Hannes Pichler, and Oskar Painter. Deterministic generation of multidimensional photonic cluster states with a single quantum emitter. *arXiv preprint arXiv:2206.10076*, 2022. URL: <https://arxiv.org/abs/2206.10076>, doi:10.48550/arXiv.2206.10076.
- [33] Peter J Shadbolt, Maria R Verde, Alberto Peruzzo, Alberto Politi, Anthony Laing, Mirko Lobino, Jonathan CF Matthews, Mark G Thompson, and Jeremy L O’Brien. Generating, manipulating and measuring entanglement and mixture with a reconfigurable photonic circuit. *Nature Photonics*, 6(1):45–49, 2012. URL: <https://www.nature.com/articles/nphoton.2011.283>, doi:10.1038/nphoton.2011.283.
- [34] Jacques Carolan, Christopher Harrold, Chris Sparrow, Enrique Martín-López, Nicholas J Russell, Joshua W Silverstone, Peter J Shadbolt, Nobuyuki Matsuda, Manabu Oguma, Mikitaka Itoh, et al. Universal linear optics. *Science*, 349(6249):711–716, 2015. URL: <https://www.science.org/doi/10.1126/science.aab3642>, doi:10.1126/science.aab3642.
- [35] Stefano Paesani, Yunhong Ding, Raffaele Santagati, Levon Chakhmakhchyan, Caterina Vigliar, Karsten Rottwitt, Leif K Oxenløwe, Jianwei Wang, Mark G Thompson, and Anthony Laing. Generation and sampling of quantum states of light in a silicon chip. *Nature Physics*, 15(9):925–929, 2019. URL: <https://www.nature.com/articles/s41567-019-0567-8>, doi:10.1038/s41567-019-0567-8.
- [36] Felix Eltes, Gerardo E Villarreal-Garcia, Daniele Caimi, Heinz Siegwart, Antonio A Gentile, Andy Hart, Pascal Stark, Graham D Marshall, Mark G Thompson, Jorge Barreto, et al. An integrated optical modulator operating at cryogenic temperatures. *Nature Materials*, 19(11):1164–1168, 2020. URL: <https://pubmed.ncbi.nlm.nih.gov/32632281/>, doi:10.1038/s41563-020-0725-5.
- [37] Cheng Wang, Mian Zhang, Xi Chen, Maxime Bertrand, Amirhassan Shams-Ansari, Sethumadhavan Chandrasekhar, Peter Winzer, and Marko Lončar. Integrated lithium niobate electro-optic modulators operating at cmos-compatible voltages. *Nature*, 562(7725):101–104, 2018. URL: <https://www.nature.com/articles/s41586-018-0551-y>, doi:10.1364/OPTICA.415762.
- [38] H Bombin, IH Kim, D Litinski, N Nickerson, M Pant, F Pastawski, S Roberts, and T Rudolph. Interleaving: Modular architectures for fault-tolerant photonic quantum computing (2021). *arXiv preprint arXiv:2103.08612*. URL: <https://arxiv.org/abs/2103.08612>, doi:10.48550/arXiv.2103.08612.
- [39] Marc Hein, Wolfgang Dür, Jens Eisert, Robert Raussendorf, M Nest, and H-J Briegel. Entanglement in graph states and its applications. *arXiv preprint quant-ph/0602096*, 2006. URL: <https://arxiv.org/abs/quant-ph/0602096>, doi:10.48550/arXiv.quant-ph/0602096.
- [40] Harry Kesten et al. The critical probability of bond percolation on the square lattice equals 1/2. *Communications in mathematical physics*, 74(1):41–59, 1980. URL: <https://link.springer.com/article/10.1007/BF01197577>, doi:10.1007/BF01197577.
- [41] Steven A Cuccaro, Thomas G Draper, Samuel A Kutin, and David Petrie Moulton. A new quantum ripple-carry addition circuit. *arXiv preprint quant-ph/0410184*, 2004. URL: <https://arxiv.org/abs/quant-ph/0410184>, doi:10.48550/arXiv.quant-ph/0410184.
- [42] Max Alteg, Baptiste Chevalier, Octave Mestoudjian, and Johan-Luca Rossi. Study of adaptative derivative-assemble pseudo-trotter ansatzes in vqe through qiskit api. 2022. arXiv:2210.15438.
- [43] Jia-Bin You, Dax Enshan Koh, Jian Feng Kong, Wen-Jun Ding, Ching Eng Png, and Lin Wu. Exploring variational quantum eigen-solver ansatzes for the long-range xy model. 2021. arXiv:2109.00288.